

# **Power Systems**

Electrical power has been the technological foundation of industrial societies for many years. Although the systems designed to provide and apply electrical energy have reached a high degree of maturity, unforeseen problems are constantly encountered, necessitating the design of more efficient and reliable systems based on novel technologies. The book series Power Systems is aimed at providing detailed, accurate and sound technical information about these new developments in electrical power engineering. It includes topics on power generation, storage and transmission as well as electrical machines. The monographs and advanced textbooks in this series address researchers, lecturers, industrial engineers and senior students in electrical engineering.


\*\* Power Systems is indexed in Scopus\*\*

More information about this series at <http://www.springer.com/series/4622>

Muhammad Ali Masood Cheema ·  
John Edward Fletcher

# Advanced Direct Thrust Force Control of Linear Permanent Magnet Synchronous Motor

Muhammad Ali Masood Cheema  
Research and Special Design  
Northern Transformer Corporation  
Maple, ON, Canada

John Edward Fletcher   
The University of New South Wales  
Sydney, NSW, Australia

ISSN 1612-1287

Power Systems

ISBN 978-3-030-40324-9

<https://doi.org/10.1007/978-3-030-40325-6>

ISSN 1860-4676 (electronic)

ISBN 978-3-030-40325-6 (eBook)

© Springer Nature Switzerland AG 2020

This work is subject to copyright. All rights are reserved by the Publisher, whether the whole or part of the material is concerned, specifically the rights of translation, reprinting, reuse of illustrations, recitation, broadcasting, reproduction on microfilms or in any other physical way, and transmission or information storage and retrieval, electronic adaptation, computer software, or by similar or dissimilar methodology now known or hereafter developed.

The use of general descriptive names, registered names, trademarks, service marks, etc. in this publication does not imply, even in the absence of a specific statement, that such names are exempt from the relevant protective laws and regulations and therefore free for general use.

The publisher, the authors and the editors are safe to assume that the advice and information in this book are believed to be true and accurate at the date of publication. Neither the publisher nor the authors or the editors give a warranty, expressed or implied, with respect to the material contained herein or for any errors or omissions that may have been made. The publisher remains neutral with regard to jurisdictional claims in published maps and institutional affiliations.

This Springer imprint is published by the registered company Springer Nature Switzerland AG  
The registered company address is: Gewerbestrasse 11, 6330 Cham, Switzerland

**To**

**“My Old Man”**

***Muhammad Masood Cheema***

*“Baba! we did it together. It is your immense love and spiritual bond I have with you that enabled me to accomplish this great achievement.”*

**To**

***Dr. Farrukh Humayun Cheema***

*“For your selfless love that always gave me strength.”*

***Dr. Muhammad Ali Masood Cheema***

**To**

*“To those who walked before me for making this research possible, and for those who will follow for their dedication and pursuit of understanding.”*

***Dr. John Edward Fletcher***

# Preface

The application areas for linear permanent magnet synchronous motors (linear PMSMs) include, but not limited to, servo-mechanisms, automation of manufacturing processes, transportation, renewable energy devices and pumping machinery. The broadening scope of the linear PMSMs implies the importance of developing robust, simple and fast control mechanisms for the linear drives to suit the essential needs of these emerging industries.

This book is focused on the direct thrust force control (DTFC) of tubular surface-mount linear PMSMs. The concept of DTFC is derived from direct torque control scheme which was first introduced in the 1980s initially for rotational induction machines, and in later studies this scheme was also applied to rotational permanent magnet synchronous motors (PMSMs). The simple structure of the direct torque control scheme provides it with inherent robustness to parameter variation and a fast transient response. These attributes make this control scheme a prime candidate when robustness and fast transient response are of vital significance. In recent years, direct torque control scheme has also been extended to linear PMSMs as DTFC; however, a little is published so far in this regard.

The DTFC scheme is analogous to direct torque control and has a similar switching table-based control structure in conjunction with two multilevel hysteresis comparators to regulate stator flux and thrust force. These hysteresis comparators are simplest form of a scaled relay controller with unity gain and are robust to parameter variation; therefore, DTFC is variable structure control scheme in nature. However, the main disadvantage of DTFC, due to the variable structure nature of the control scheme, is the presence of ripple in the stator flux and thrust force and a variable switching frequency.

The implementation of DTFC for linear PMSMs is substantially challenging compared to direct torque control of rotational PMSMs. In general, most of the linear PMSMs have a low value of stator inductance due to their larger air gap compared to rotational PMSMs. Also, due to the linear motion, the pole pitch of the linear PMSMs also affects the thrust force regulation. Therefore, classical switching table-based DTFC-controlled linear PMSMs with low inductance and short pole pitch exhibit large thrust force ripple which is typically beyond acceptable limits.

This book aims at in-depth formulation of nonlinear dynamic models for linear permanent magnet synchronous motors from a control system perspective and subsequently utilizes these models to develop several advanced DTFC schemes based on optimal control and sliding mode control approaches. A detailed chapter is also dedicated to formulation of sliding mode stator flux observer for sensorless speed estimation of linear PMSM. It is worth mentioning that extensive experimental results based on a laboratory prototype for validation of the presented control schemes along with exhaustive discussions are included in the text as well.

Chapters 1 and 2 of the book are based on a detailed literature review and comprehensive mathematical modelling of linear PMSMs in various reference frames. The conventional switching table-based DTFC is analysed at length in Chap. 3. In order to reduce the ripple and steady-state error in the stator flux and thrust force response of the linear PMSM, a duty ratio control-based control is proposed and studied to adapt switching table-based DTFC as provided in Chap. 3 of the book.

Another approach to effectively reduce steady-state thrust force ripple is to use space vector pulse-width modulation approach. In Chaps. 4–7, several advanced DTFC schemes utilizing space vector pulse-width modulation are proposed and analysed. Finally, a stator flux observer for sensorless speed estimation comprising a linear state observer and an improved sliding mode component is also proposed in Chap. 7.

The key feature of this book is formulation of a nonlinear second-order state-space model of the linear PMSM in a synchronously rotating stator flux vector  $xy$ -reference frame for combined dynamics of speed and thrust force as system states. The proposed nonlinear model is used to formulate the sliding mode control law with space vector pulse-width modulation for combined control of speed and thrust force.

In view of this fact that this text is written in way that the development of advanced concepts stems from a detailed mathematical foundation of the subject matter, this book is a suitable choice to be used as textbook or reference for undergraduate/graduate students for the subject of advanced electrical drives.

It is important to note that, although this book is set in the context of linear PMSMs, however the concepts and mathematical formulations presented here can conveniently be adapted or generalized for direct torque control for rotational multiphase PMSMs with or without saliency. This can be of great help for graduate research students and professional engineers in the field of electrical drives to expand their understanding of advanced nonlinear dynamics and control schemes for linear/rotational PMSMs.

Maple, Canada  
Sydney, Australia

Muhammad Ali Masood Cheema  
John Edward Fletcher

# Acknowledgements

The core of this book is based on my doctoral and postdoctoral research under the supervision of Prof. John Edward Fletcher and co-supervision of Prof. Muhammad Fazlur Rahman.

First and foremost, I want to express my gratitude to my supervisors, Prof. John Edward Fletcher and Prof. Muhammad Fazlur Rahman of the Energy Systems Research Group at the University of New South Wales, for their guidance and support throughout the course of my research for this book. I will always cherish my time that I spent under supervision of Prof. John Edward Fletcher who has always been kind to me and provided me the opportunity for this research.

I also thank the University of New South Wales and the Faculty of Engineering for providing the scholarship that enabled the research for this book and also for conferring on me the title of adjunct lecturer that allowed me to further advance the research for this book.

I also wish to acknowledge valuable support and financial assistance from the management of Northern Transformer Corporation (NTC) who facilitated me in writing this manuscript. I wish to express my gratitude to Alexei Miecznikowski, CEO of NTC, who has been very supportive throughout the course of this book and encouraged me to push the envelope in research.

I would also like to thank the technical staff in the energy system research group of UNSW for their support in logistics. Special thanks to Dr. Dan Xiao and Mr. Gamini Liyadipitiya for their assistance in the experimental work vital to conclude this book. I would also like to thank Mr. Merlin Chai, Mr. Kazi Ahsanullah and Mr. David Tan for their insightful discussion and suggestions.

I wish to pay special thanks to my friend Dr. Mohammad Farashadnia for his valuable support throughout the duration of this research. I am also grateful to my brother Muhammad Ammar Masood Cheema for his love and support during my studies and always being my strength to fight my forward in the life.

I am greatly indebted to my parents and sister for their endless love, continuous encouragement, spiritual and financial support during my studies leading to this book. My father Engr. Muhammad Masood Cheema and mother Dr. Fozia have



played a pivotal role throughout in my life, and it is their immense love and faith in myself that enabled me to accomplish this task and made me the person I am today. I am very fortunate to have Dr. Farrukh Humayun Cheema and Najma Farrukh also as my parents who selflessly loved me, supported me and stood strong by me throughout my life; without them, this book would have been a far-fetched dream.

I wish to express my love and gratitude to my wife Sunbal for standing by my side during my Ph.D. studies. Wify! you have always been there for me.

Lastly, I wish to express love for my sons Muhammad Ali Murtaza and Muhammad Ali Mujtaba who have always been a source of great motivation and joy in my life.

Dr. Muhammad Ali Masood Cheema

# Contents

<b>1</b>	<b>Introduction</b>	1
1.1	Motivation and Scope	1
1.2	Types of Linear Permanent Magnet PMSMs	2
1.3	A Review of Developments in Direct Thrust Force Control of Linear PMSM	2
1.4	Description of Experimental Setup	7
1.5	Book Outline	8
1.6	Conclusions	9
	References	9
<b>2</b>	<b>Mathematical Modeling of Surface-Mount Linear Permanent Magnet Synchronous Motor</b>	13
2.1	Introduction	13
2.2	Construction of Tubular Surface-Mount Linear PMSM	14
2.3	Dynamic Modeling of Surface-Mount Linear PMSM in 3-Phase Stationary $abc$ -Reference Frame	15
2.3.1	Mapping of Three-Phase Machine Variables to Complex Space Vectors	19
2.4	Two-Axis Dynamic Models of Linear PMSM	27
2.4.1	Dynamic Model of Linear PMSM in the $dq$ -Reference Frame	28
2.4.2	Dynamic Model of Linear PMSM in $\alpha\beta$ -Reference Frame	34
2.4.3	Dynamic Model of Linear PMSM in $xy$ -Reference Frame	38
2.5	Estimation of Stator Flux Magnitude and Thrust Force Base on $Dq$ -Axes Current Model	41
2.6	Conclusion	42
	References	42

<b>3</b>	<b>Direct Thrust Force Control Based on Duty Ratio Control</b>	45
3.1	Introduction	45
3.2	Basic Principle of Direct Thrust Force Control	45
3.2.1	Selection of Reference Stator Flux Magnitude $\lambda_{ref}$	48
3.2.2	Operational Range of Load Angle $\delta$ for Low Inductance Surface-Mount Linear PMSM	48
3.3	Stability Analysis of Direct Thrust Force Control	49
3.3.1	Lyapunov Stability Analysis of Conventional DTFC	50
3.4	Effect of Inverter Voltage Vectors on Thrust Force and Flux Variation	52
3.5	Experimental Results for Conventional DTFC	57
3.6	Duty Ratio Control	59
3.7	Review of Classical Duty Ratio Control Methods	60
3.8	State of the Art Duty Ratio Control Method	62
3.8.1	Tuning of Static Gains $C_T$ and $C_F$	62
3.9	Proposed Duty Ratio Control Method	63
3.9.1	Derivation of Expression for $\Delta F_T$	65
3.9.2	Derivation of Expression for $\Delta \lambda_s$	66
3.9.3	Derivation of Expressions for $d_F$ and $d_\lambda$	66
3.10	Experimental Results for Duty Ratio Controlled DTFC	67
3.10.1	Start-Up Performance with Speed Loop Closed	67
3.10.2	Speed Reversal and Steady-State Performance	70
3.10.3	Analysis of Steady State Error in Force for DTFC1	77
3.10.4	Flux Trajectory	78
3.10.5	Transient Response of Force with Outer Speed Loop Disabled	79
3.11	Conclusions	79
	References	80
<b>4</b>	<b>SV-PWM Based Direct Thrust Force Control of a Linear Permanent Magnet Synchronous Motor</b>	83
4.1	Introduction	83
4.2	Stator Flux and Thrust Force Regulation in $\alpha\gamma$ -Reference Frame	84
4.3	Analysis of Thrust Force Control in Surface-Mount Linear PMSM	84
4.3.1	Selection of Reference Stator Flux Magnitude $\lambda_{ref}$	85
4.3.2	Characteristics of the Co-efficient $K$ for Surface-Mount Linear PMSM with Low Stator Inductance and Short Pole-Pitch	86
4.4	Derivation of Transfer Function for Stator Flux Regulation	88
4.5	Derivation of Transfer Function for Thrust Force Regulation	88
4.6	PI Controller Based Direct Thrust Force Control (PI-DTFC)	90

- 4.6.1 Stator Flux Control Loop . . . . . 91
- 4.6.2 Thrust Force Control Loop . . . . . 95
- 4.6.3 Discrete Time Design of Stator Flux and Force PI  
Controllers . . . . . 99
- 4.7 Linear Quadratic Regulator Based Direct Thrust Force Control  
of Linear PMSM (Optimal-DTFC1) . . . . . 115
  - 4.7.1 Formulation of a Novel State Space Model of the  
Linear PMSM . . . . . 115
  - 4.7.2 Controllability of the Novel State Space Model . . . . . 117
- 4.8 Linear Quadratic Regulator Based State Feedback Control  
with Integral Action . . . . . 117
  - 4.8.1 Mathematical Formulation of Error Dynamics . . . . . 118
  - 4.8.2 Optimal Linear Quadratic Regulator Design . . . . . 120
- 4.9 Novel LQR Based Direct Thrust Force Control  
of the Linear-PMSM . . . . . 121
  - 4.9.1 Controllability Analysis of the Error Dynamics . . . . . 122
  - 4.9.2 Choice of Gain Matrix for State Feedback Law . . . . . 122
- 4.10 Experimental Validation of Proposed Control Scheme . . . . . 123
  - 4.10.1 Dynamic Response with Outer Speed Loop Disabled . . . . . 124
  - 4.10.2 Steady-State Regulation with Outer Speed Loop  
Disabled . . . . . 126
  - 4.10.3 Start-Up Speed Response with Outer Speed Loop  
Enabled . . . . . 127
  - 4.10.4 Speed Reversal with Outer Speed Loop Enabled . . . . . 129
  - 4.10.5 Steady-State Response with Outer Speed Loop  
Enabled . . . . . 129
- 4.11 Conclusions . . . . . 132
- References . . . . . 132
- 5 Optimal, Combined Speed and Direct Thrust Force Control  
of a Linear Permanent Magnet Synchronous Motors . . . . . 135**
  - 5.1 Introduction . . . . . 135
  - 5.2 State Space Model of the Linear PMSM in the  $xy$ -Reference  
Frame for Combined Flux, Thrust and Speed Dynamics . . . . . 136
    - 5.2.1 Controllability Analysis of the Novel State Space  
Model . . . . . 139
  - 5.3 Linear Quadratic Regulator Based State Feedback Control  
with Integral Action . . . . . 139
    - 5.3.1 Mathematical Formulation of Error Dynamics . . . . . 140
    - 5.3.2 Formulation of the Linear Quadratic Regulator . . . . . 142

5.4	Linear Quadratic Regulator Based Combined Speed and Direct Thrust Control . . . . .	143
5.4.1	Controllability Analysis of the Error Dynamics . . . . .	145
5.4.2	Choice of Gain Matrix for State Feedback Law . . . . .	145
5.5	Experimental Validation of Proposed Optimal-DTFC2 . . . . .	146
5.5.1	Start-Up Speed Response . . . . .	146
5.5.2	Speed Reversal and Steady-State Response . . . . .	149
5.5.3	Effect of Parameter Variation on the Performance . . . . .	152
5.6	Conclusions . . . . .	153
	References . . . . .	153
<b>6</b>	<b>Sliding Mode Based Combined Speed and Direct Thrust Force Control of a Linear Permanent Magnet Synchronous Motors . . . . .</b>	<b>155</b>
6.1	Introduction . . . . .	155
6.2	Dynamic Model of the Linear PMSM in $xy$ -Reference Frame . . . . .	155
6.3	Sliding Mode Control . . . . .	158
6.3.1	Fundamentals of Sliding Mode Control . . . . .	158
6.3.2	Variable Structure Based Direct Torque Control . . . . .	162
6.4	Sliding Mode Control with Augmented Integral Action . . . . .	163
6.4.1	Sliding Surface for Stator Flux Regulation . . . . .	164
6.4.2	Sliding Surface for Speed Regulation . . . . .	165
6.4.3	Control Law for Stator Flux Regulation . . . . .	165
6.4.4	Control Law for Combined Speed and Thrust Force Regulation . . . . .	166
6.4.5	Chattering Reduction . . . . .	169
6.5	Experimental Validation of Proposed SM-DTFC1 . . . . .	169
6.5.1	Start-Up Speed Response . . . . .	170
6.5.2	Speed Reversal and Steady-State Response . . . . .	172
6.5.3	Evaluation of Robustness to the Parameter Variation . . . . .	176
6.6	Conclusions . . . . .	177
	References . . . . .	178
<b>7</b>	<b>Sensorless Control of a Linear Permanent Magnet Synchronous Motors Using a Combined Sliding Mode Adaptive Observer . . . . .</b>	<b>181</b>
7.1	Introduction . . . . .	181
7.2	Dynamic State Space Model of Linear PMSM in $xy$ -Reference Frame . . . . .	182
7.3	Combined Speed and Direct Thrust Force Control of Linear PMSM Based on Integral Sliding Mode Control . . . . .	184
7.3.1	Sliding Surface for Stator Flux Regulation . . . . .	185
7.3.2	Sliding Surface for Speed Regulation . . . . .	185
7.3.3	Control Law for Stator Flux Regulation . . . . .	185
7.3.4	Control Law for Thrust Force Regulation . . . . .	186

- 7.4 A Novel Combined Sliding Mode State Observer . . . . . 189
  - 7.4.1 Stability Analysis of the Proposed Observer. . . . . 191
  - 7.4.2 Gain Selection for the Proposed Observer . . . . . 192
  - 7.4.3 Adaption Scheme for Speed Estimation . . . . . 194
  - 7.4.4 Estimation of Stator Flux Magnitude  
and Thrust Force . . . . . 194
- 7.5 Experimental Results . . . . . 195
- 7.6 Experimental Evaluation of the Control Performance  
of SM-DTFC2 . . . . . 196
  - 7.6.1 Start-Up Response . . . . . 196
  - 7.6.2 Speed Reversal Response . . . . . 198
  - 7.6.3 Robustness to Parameter Variation . . . . . 201
- 7.7 Experimental Evaluation of the SM-Observer . . . . . 201
  - 7.7.1 Speed Reversal Response . . . . . 201
  - 7.7.2 Speed Reversal Response Without the Improved  
SM Function . . . . . 203
  - 7.7.3 Steady State Response . . . . . 203
  - 7.7.4 Position Estimation. . . . . 204
  - 7.7.5 Flux Estimation . . . . . 205
- 7.8 Conclusion . . . . . 206
- References . . . . . 206
- 8 Conclusions and Future Work . . . . . 209**
  - 8.1 Conclusions . . . . . 209
  - 8.2 Main Contributions of the Book. . . . . 211
  - 8.3 Future Work . . . . . 213
- Appendix A: Description of the Experimental Setup . . . . . 215**
- Appendix B: Derivation of Expressions for  $\frac{dF_T}{dt}$  and  $\frac{d\lambda_s}{dt}$ . . . . . 221**

# List of Figures

Fig. 1.1	Schematic diagram of experimental setup showing the prototype linear PMSM, voltage source inverter and the control circuitry . . . . .	7
Fig. 2.1	Schematic diagram of a tubular surface-mount linear PMSM . . . . .	14
Fig. 2.2	Schematic diagram of the three-phase winding configuration for the linear PMSM. The orientation of the windings is arbitrarily shown and does not correspond to the physical magnetic axes of the machine as in the usual case of rotational machine [9, 10] . . . . .	15
Fig. 2.3	Space vector representation of stator phase voltages, <b>a</b> voltage space vector (green) and phase voltage vectors (blue), <b>b</b> synthesis of voltage space vector according to Eq. (2.18). . . . .	20
Fig. 2.4	Illustration and angular orientations and of stator current, permanent magnet flux linkage, and stator flux linkage space vectors stationary <i>abc</i> -reference frame. All the angles are measured from <i>a</i> -axis. . . . .	23
Fig. 2.5	Steady-state space vector diagram of the linear PMSM in stationary <i>abc</i> -reference frame according to Eq. (2.49). The length of all the space vectors is arbitrarily shown . . . . .	27
Fig. 2.6	The stator and mover's flux linkages in various reference frames . . . . .	28
Fig. 2.7	Equivalent circuit of the tubular surface-mount linear PMSM, <b>a</b> <i>d</i> -axis Equivalent circuit according to Eq. (2.72), <b>b</b> <i>q</i> -axis Equivalent circuit according to Eq. (2.73) . . . . .	32
Fig. 2.8	Steady-state space vector diagram of the linear PMSM in <i>dq</i> -reference frame as Eq. (2.80). The length of all the space vectors are arbitrarily shown . . . . .	33
Fig. 2.9	Steady-state space vector diagram of the linear PMSM in <i>xy</i> -reference frame according to Eq. (2.131). The length of all the space vectors is arbitrarily shown . . . . .	36

Fig. 2.10 Steady-state space vector diagram of the linear PMSM in  $xy$ -reference frame when the resistive drop  $R_s \vec{I}_s$  is neglected. The length of all the space vectors is arbitrarily shown . . . . . 41

Fig. 3.1 Voltage space vectors generated by a 2-level VSI [5, 6] and control of magnitude and rotation of stator flux vector. Note the magnitude variation of stator flux is kept within the hysteresis band (diagram is not to scale) . . . . . 47

Fig. 3.2 Block diagram of the conventional DTFC scheme . . . . . 47

Fig. 3.3 Rate of change of stator flux for active ( $V_1$  to  $V_6$ ) and zero ( $V_0$  and  $V_7$ ) voltage vectors ( $v_m = 600$  mm/s and operating thrust force  $F_0 = 53$  N) . . . . . 54

Fig. 3.4 Rate of change of thrust force for active ( $V_1$  to  $V_6$ ) and zero ( $V_0$  and  $V_7$ ) voltage vectors ( $v_m = 600$  mm/s and operating thrust force  $F_0 = 53$  N) . . . . . 55

Fig. 3.5 Variation in stator flux for active ( $V_1$  to  $V_6$ ) and zero ( $V_0$  and  $V_7$ ) voltage vectors during one sampling period  $T_s = 100 \mu s$  ( $v_m = 600$  mm/s and operating thrust force  $F_0 = 53$  N) . . . . . 56

Fig. 3.6 Variation in thrust force for active ( $V_1$  to  $V_6$ ) and zero ( $V_0$  and  $V_7$ ) voltage vectors during one sample time  $T_s = 100 \mu s$  ( $v_m = 600$  mm/s and operating thrust force  $F_0 = 53$  N) . . . . . 56

Fig. 3.7 Variation in peak value of the negative rate of change of thrust force  $\frac{dF_r}{dt}$ , caused by any of the zero voltage vectors ( $V_0$  and  $V_7$ ), at different speed for various values of operating thrust force  $F_0$  . . . . . 57

Fig. 3.8 Variation in the peak value of positive rate of change of thrust force  $\frac{dF_r}{dt}$ , caused by any of the active voltage vectors ( $V_1$  to  $V_6$ ), at different speed for various values of operating thrust force  $F_0$  . . . . . 57

Fig. 3.9 From top to bottom, speed response, thrust force response, flux response, and stator phase  $a$  current response under conventional DTFC. **a** Start-up from 0 to 200  $\text{mms}^{-1}$ , **b** speed reversal from  $-600$  to 600 mm/s (experiment) . . . . . 58

Fig. 3.10 Illustration of duty ratio control, the active voltage vector is applied at the beginning of the sample time for a duration  $t_1$  followed by a zero vector applied for the rest of the sampling period  $T_s$ .  $s_1$  is the thrust force slope (rate of change) when active voltage vector is applied and  $s_2$  the thrust force slope (rate of change) when zero voltage vector is applied (diagram not to scale) . . . . . 59

Fig. 3.11 Block Diagram of the duty ratio controlled DTFC scheme, duty ratio is computed using (3.52) for the state of the art [39] and for proposed method (3.56) is used . . . . . 62



Fig. 3.12 Illustration of proposed duty ratio control, the active voltage vector is applied at the beginning of the sample time for duration  $t_1$  followed by a zero vector applied for the rest of the sampling period  $T_s$ . Dotted line shows the variation in thrust force if the active vector would have been applied for full sampling period (diagram not to scale) . . . . . 63

Fig. 3.13 Start-up performance from 0 to 80 mm/s with outer speed loop closed. Speed, force, flux, duty ratio and stator phase currents responses are shown from top to bottom respectively for both the DTFC1 ( $C_T = 120$  N,  $C_F = 3$  Wb) and the novel DTFC (experiment). . . . . 68

Fig. 3.14 Magnified view of the speed response during start-up. **a** DTFC1 ( $C_T = 120$  N,  $C_F = 3$  Wb), **b** novel DTFC (experiment). . . . . 69

Fig. 3.15 Error plots for speed and thrust force during startup transient. **a** DTFC1 ( $C_T = 120$  N,  $C_F = 3$  Wb) and, **b** novel DTFC (experiment). . . . . 69

Fig. 3.16 Speed reversal from  $-600$  to  $600$  mm/s and steady-state response at  $600$  mm/s with outer speed loop closed. Speed, force, flux, duty ratio and stator phase  $a$  current responses are shown from top to bottom respectively for both the DTFC1 ( $C_T = 120$  N,  $C_F = 3$  Wb) and novel DTFC (experiment) . . . . . 71

Fig. 3.17 Magnified view of the speed reversal transient illustrating the rise times. **a** DTFC1 ( $C_T = 120$  N,  $C_F = 3$  Wb) and, **b** novel DTFC (experiment) . . . . . 72

Fig. 3.18 Error plots for speed during speed reversal transient. **a** DTFC1 ( $C_T = 120$  N,  $C_F = 3$  Wb) and, **b** novel DTFC (experiment). . . . . 72

Fig. 3.19 Thrust force response during steady-state at  $600$  mm/s, **a** DTFC1 ( $C_T = 120$  N,  $C_F = 3$  Wb) and, **b** novel DTFC (experiment). . . . . 74

Fig. 3.20 Duty-ratio  $d_F$ , force error  $e_F$ ,  $C_T$  for DTFC 1 ( $C_T = 120$  N,  $C_F = 3$  Wb) and  $\Delta F_T$  for novel DTFC (experiment). **a** Whole duration of steady-state from  $0.3$  to  $0.7$  s. **b** Magnification to  $10$  sampling periods from  $0.35$  to  $0.351$  s, each time division is equal to  $2.5$  sampling periods. . . . . 75

Fig. 3.21  $\alpha\beta$ -axes stator voltages, currents and flux components during steady-state at  $600$  mm/s, **a** DTFC1 ( $C_T = 120$  N,  $C_F = 3$  Wb) and, **b** novel DTFC (experiment). . . . . 76

Fig. 3.22 Variation in average steady-state error and percent ripple in force with speed for both DTFC1 ( $C_T = 120$  N,  $C_F = 3$  Wb) and the novel DTFC . . . . . 77

Fig. 3.23 Flux trajectories at various speeds (experiment). . . . . 78

Fig. 3.24 Transient response of force under the DTFC1 (experiment). . . . . 79

Fig. 3.25	Transient response of force under the novel DTFC (experiment) . . . . .	80
Fig. 4.1	Thrust force versus load angle for the surface-mount linear PMSM of Table 1.1, the exact curve is according to (4.5) and the linearized curve is according to (4.6) with $\lambda_s = 0.0846$ Wb, according to (4.7) under (MFPA) . . . . .	87
Fig. 4.2	Characteristics of $K$ according to (4.10) with $\lambda_s = 0.0846$ Wb . . . . .	87
Fig. 4.3	Block diagram of stator flux regulation according to (4.11) . . . . .	88
Fig. 4.4	Block diagram of thrust force regulation according to (4.20) . . . . .	90
Fig. 4.5	PI controller based direct thrust force control (PI-DTFC) of the linear PMSM with space vector pulse width modulation (SV-PWM) . . . . .	90
Fig. 4.6	Block diagram of the stator flux control loop with transport delay and disturbance cancellation (4.11) and (4.26) . . . . .	91
Fig. 4.7	Block diagram of the thrust force control loop with transport delay and disturbance cancellation (4.20) and (4.50) . . . . .	96
Fig. 4.8	Discrete time stator flux control loop for the surface-mount linear PMSM . . . . .	100
Fig. 4.9	The root locus and the selected closed loop poles for the stator flux controller loop . . . . .	104
Fig. 4.10	Discrete time thrust force control loop for the linear PMSM . . . . .	106
Fig. 4.11	The root locus and the selected closed loop poles for the thrust force control loop . . . . .	109
Fig. 4.12	Open loop frequency response of the thrust force control loop . . . . .	110
Fig. 4.13	Force step response with corresponding error plots for different values of the damping ratio $\xi_d$ : <b>a</b> $\xi_d = 0.95$ , <b>b</b> $\xi_d = 0.9$ , <b>c</b> $\xi_d = 0.707$ , <b>d</b> $\xi_d = 0.50$ (experiment, reference force is shown in red and estimated force is shown in green) . . . . .	111
Fig. 4.14	Open loop frequency response of thrust force control loop for various values of stator resistance $R_s$ . ( $\xi_d = 0.95$ , $k_{p\_F} = 0.0480$ , and $k'_{i\_F} = 0.0174$ ) . . . . .	112
Fig. 4.15	PI controller with output limiter . . . . .	113
Fig. 4.16	PI controller with limited output and anti-windup scheme for the integrator [11]. . . . .	113
Fig. 4.17	Implementation of the voltage limiter for the PI controller. . . . .	114
Fig. 4.18	Type-0 servo system with full state feedback and integral action . . . . .	117

Fig. 4.19 Proposed linear quadratic regulator based direct thrust control (Optimal-DTFC1) of linear PMSM, the integral action is added by state augmentation. . . . . 118

Fig. 4.20 Force step response of PI-DTFC (experiment). . . . . 125

Fig. 4.21 Force step response of Optimal-DTFC1. . . . . 126

Fig. 4.22 From top to bottom the force response, magnified force response, steady-state error in the force and steady-state stator flux response is shown, **a** PI-DTFC, and **b** Optimal-DTFC1 . . . 127

Fig. 4.23 Start-up performance from 0 to 200 mm/s with outer speed loop closed. Speed, force, stator flux, and stator phase currents responses are shown from top to bottom respectively for both **a** the PI-DTFC and **b** Optimal-DTFC1 (experiment) . . . . . 128

Fig. 4.24 Magnified view of the speed response during start-up, **a** PI-DTFC, and **b** Optimal-DTFC1 (experiment). . . . . 128

Fig. 4.25 Speed reversal from -600 to 600 mm/s and steady-state response at 600 mm/s with outer speed loop closed. Speed, force, stator flux, duty ratio and stator phase *a* current responses are shown from top to bottom respectively for both **a** the PI-DTFC and **b** Optimal-DTFC1 (experiment) . . . . . 130

Fig. 4.26 Magnified view of the speed reversal transient **a** PI-DTFC, and **b** Optimal-DTFC1 (experiment) . . . . . 131

Fig. 4.27 Steady-state performance at 600 mm/s. From top, speed, force, and stator flux responses are shown for both **a** the PI-DTFC and **b** Optimal-DTFC1 (experiment) . . . . . 131

Fig. 5.1 Type-0 servo system with full state feedback and integral action . . . . . 140

Fig. 5.2 Proposed linear quadratic regulator based combined speed and thrust control of linear PMSM, the integral action is added by state augmentation. . . . . 140

Fig. 5.3 Start-up performance from 0 to 200 mm/s. Speed, thrust force, stator flux, and stator phase currents responses are shown from top to bottom respectively for both **a** the PI-DTFC and **b** optimal-DTFC2 (experiment). . . . . 147

Fig. 5.4 Magnified view of the speed response during start-up, **a** PI-DTFC, and **b** optimal-DTFC2 (experiment) . . . . . 148

Fig. 5.5 Magnified view of the speed response during start-up, **a** PI-DTFC, and **b** optimal-DTFC2 (experiment) . . . . . 148

Fig. 5.6 Magnified thrust force response during start-up, **a** PI-DTFC, and **b** optimal-DTFC2 (experiment) . . . . . 148

Fig. 5.7 Speed reversal from -600 to 600 mm/s and steady-state response at 600 mm/s. Speed, force, flux, and stator phase “*a*” current responses are shown, **a** PI-DTFC, and **b** optimal-DTFC2 (experiment) . . . . . 150

Fig. 5.8	Magnified view of the speed reversal transient, <b>a</b> PI-DTFC, and <b>b</b> optimal-DTFC2 (experiment) . . . . .	150
Fig. 5.9	Error plots for the speed response during speed reversal transient, <b>a</b> PI-DTFC, and <b>b</b> Optimal-DTFC2 (experiment) . . . .	151
Fig. 5.10	Steady-state performance at 600 mm/s. Speed, thrust force, and stator flux responses are shown, <b>a</b> PI-DTFC, and <b>b</b> optimal-DTFC2 (experiment) . . . . .	151
Fig. 5.11	Effect of parameter variation on the transient performance of optimal-DTFC2 during speed reversal from $-600$ to $600$ mm/s, <b>a</b> $R_s$ is increased by 100%, <b>b</b> $L_s$ is increased by 100% (experiment) . . . . .	152
Fig. 6.1	Schematics describing the sliding mode control with first order plus integral sliding condition for non-linear combined speed and thrust force dynamics proposed in (6.5) and (6.5a) . . . . .	169
Fig. 6.2	Proposed sliding mode based combined speed and thrust control of linear PMSM (SM-DTFC), the integral action is added by modification of the reachability condition . . . . .	170
Fig. 6.3	Start-up performance from 0 to 200 mm/s. Speed, thrust force, stator flux, and stator phase currents responses are shown from top to bottom respectively for both <b>a</b> the PI-DTFC and <b>b</b> SM-DTFC1 (experiment) . . . . .	171
Fig. 6.4	Magnified view of the speed response during start-up, <b>a</b> PI-DTFC, and <b>b</b> SM-DTFC1 (experiment) . . . . .	171
Fig. 6.5	Magnified view of the speed error during start-up, <b>a</b> PI-DTFC, and <b>b</b> SM-DTFC1 (experiment) . . . . .	172
Fig. 6.6	Magnified thrust force response during start-up, <b>a</b> PI-DTFC, and <b>b</b> SM-DTFC1 (experiment) . . . . .	172
Fig. 6.7	Speed reversal from $-600$ to $600$ mm/s and steady state response at 600 mm/s. Speed, force, flux, and stator phase “ $a$ ” current responses are shown, <b>a</b> PI-DTFC, and <b>b</b> SM-DTFC1 (experiment) . . . . .	173
Fig. 6.8	Magnified view of the speed reversal transient, <b>a</b> PI-DTFC, and <b>b</b> SM-DTFC1 (experiment) . . . . .	173
Fig. 6.9	Error plots for the speed response during the speed reversal transient, <b>a</b> PI-DTFC, and <b>b</b> SM-DTFC1 (experiment) . . . . .	174
Fig. 6.10	Steady state performance at 600 mm/s. Speed, thrust force, and stator flux responses are shown, <b>a</b> PI-DTFC, and <b>b</b> SM-DTFC1 (experiment) . . . . .	175
Fig. 7.1	Schematic illustration of the non-linear combined speed and thrust force dynamics proposed in (7.2) and (7.2a) and the proposed sliding mode control with integral action of (7.31) . . . . .	189
Fig. 7.2	Block diagram of proposed observer . . . . .	190
Fig. 7.3	Block diagram illustration of improved “ $sgn_m$ ” function . . . . .	191

Fig. 7.4 Block diagram of the proposed combined sliding mode speed and direct thrust control of linear PMSM with the novel adaptive observer . . . . . 195

Fig. 7.5 Startup performance from 0 to 200 mm/s. Measured Speed, thrust force, stator flux, and stator phase currents responses are shown from top to bottom respectively. **a** PI-DTFC and **b** SM-DTFC2 (experiment) . . . . . 197

Fig. 7.6 Magnified view of the measured speed and thrust force response during start-up. **a** PI-DTFC and **b** SM-DTFC2 (experiment) . . . . . 198

Fig. 7.7 Error plots for speed start-up. **a** PI-DTFC and **b** SM-DTFC (experiment) . . . . . 198

Fig. 7.8 Speed reversal from -600 to 600 mm/s and steady-state response at 600 mm/s. Measured and estimated Speed, thrust force, stator flux, duty ratio and stator phase “a” current responses are shown from top to bottom. **a** PI-DTFC and **b** SM-DTFC2 (experiment) . . . . . 199

Fig. 7.9 Magnified view of the measured and estimated speed response during start-up. **a** PI-DTFC and **b** SM-DTFC (experiment) . . . . . 199

Fig. 7.10 Magnified view of the measured and estimated speed response during steady-state. **a** PI-DTFC and **b** SM-DTFC2 (experiment) . . . . . 200

Fig. 7.11 Command voltage  $v_y$  to control thrust force, generated by the PI-DTFC and the proposed SM-DTFC2. **a** Start-up and **b** Speed reversal (experiment) . . . . . 200

Fig. 7.12 Integral sliding surface  $s_v$  according to (7.7). **a** Start-up and **b** Speed reversal (experiment) . . . . . 201

Fig. 7.13 Speed reversal response. From top speed response, speed error, thrust force and stator flux, **a** -200 to 200 mm/s, **b** -600 to 600 mm/s (experiment) . . . . . 202

Fig. 7.14 Speed reversal response without the sliding mode component. From top, speed response, speed error, and flux responses are shown, **a** -200 to 200 mm/s, **b** -600 to 600 mm/s (experiment) . . . . . 203

Fig. 7.15 Steady-state response. From top, speed response, speed error, thrust force and stator flux are shown, **a** 200 mm/s, **b** 600 mm/s (experiment) . . . . . 204

Fig. 7.16 Position estimation. **a** 200 mm/s, **b** 600 mm/s (experiment) . . . . . 205

Fig. 7.17  $\lambda_d$  and  $\lambda_q$  estimation errors with sliding mode component (novel) and without sliding mode component (linear), **a** 200 mm/s, **b** 600 mm/s (experiment) . . . . . 206

Fig. A.1 Experimental setup. . . . . 216  
Fig. A.2 Schematic circuit diagram of voltage sensing board. . . . . 217  
Fig. A.3 Schematic circuit diagram of current sensing board. . . . . 218  
Fig. A.4 Architectural overview of DS 1104 controller board. . . . . 219

# List of Tables

Table 1.1	Parameters of the prototype tubular surface-mount linear PMSM . . . . .	7
Table 3.1	Switching table to generate $V_k$ for DTFC [13]. . . . .	46
Table 3.2	$\alpha\beta$ -components of inverter voltage vectors . . . . .	54
Table 3.3	Comparison of transient performance of DTFC1 and the novel DTFC using IAE index . . . . .	70
Table 3.4	Comparison of steady-state performances of the DTFC1 for various values of $C_F$ and $C_T$ with the novel DTFC . . . . .	73
Table 4.1	Comparison of phase margin $\phi_m$ , crossover frequency, $\omega_c$ and closed loop bandwidth $\omega_b$ for various values of damping ratio $\xi_d$ . . . . .	109
Table 4.2	Comparison of force step response for various values of the damping ratio $\xi_d$ . . . . .	111
Table 4.3	Comparison of phase margin $\phi_m$ , crossover frequency $\omega_c$ and closed loop bandwidth $\omega_b$ for various values of stator resistance $R_s = 3.01 \Omega$ . . . . .	112
Table 4.4	Controller gains used in experiment for the performance comparison of Optimal-DTFC1 and PI-DTFC . . . . .	123
Table 4.5	Comparison of rise time, percent overshoot, and percent steady-state ripple in the response of thrust force PI controller under PI-DTFC for various damping ratios . . . . .	125
Table 4.6	Comparison of steady-state performance of PI-DTFC and the Optimal-DTFC1 . . . . .	131
Table 5.1	Controller gains used in experiment for the optimal-DTFC2 and PI-DTFC . . . . .	146
Table 5.2	Comparison of transient performance of PI-DTFC and the optimal-DTFC2 using IAE index . . . . .	148
Table 5.3	Comparison of steady-state performance of DTFC1 and the optimal DTFC at 600 mm/s . . . . .	152
Table 6.1	Comparison of transient performance of PI-DTFC and the SM-DTFC1 using IAE index . . . . .	172

Table 6.2	Comparison of steady state performance of PI-DTC and the SM-DTFC1 at 600 mm/s, 52 N . . . . .	175
Table 6.3	Comparison of rise time of PI-DTFC, optimal-DTFC2, and SM-DTFC1 with variation in $R_s$ . . . . .	176
Table 6.4	Comparison of rise time of PI-DTFC, optimal-DTFC2, and SM-DTFC1 with variation in $L_s$ . . . . .	176
Table 6.5	Comparison of steady-state performance of PI-DTFC, Optimal-DTFC2, and SM-DTFC1 with variation in $L_s$ . . . . .	177
Table 7.1	Controller gains used for proposed SM-DTFC2. . . . .	196
Table 7.2	Controller gains used in experiment for PI-DTFC . . . . .	196
Table 7.3	Comparison of Transient Performance of PI-DTFC and the SM-DTFC Using IAE Index . . . . .	198
Table 7.4	Comparison of steady-state performance of PI-DTFC and the SM-DTFC2. . . . .	200
Table 7.5	Comparison of robustness to parameter variation, increase in speed ripple for PI-DTFC and SM-DTFC2 . . . . .	201
Table 8.1	Comparison of transient performance in terms of rise time of PI-DTFC, optimal-DTFC1, optimal-DTFC2, and SM-DTFC1 using IAE index. . . . .	213
Table 8.2	Comparison of steady-state performance of PI-DTFC, optimal-DTFC1, optimal-DTFC2 and SM-DTFC1. . . . .	213
Table A.1	Technical specifications of the DS1104 controller board . . . . .	219